Supporting Information for

Synergistic modulation of electronic and acid-base properties of loaded Pt-Fe-Zr oxide catalyst for ethylbenzene oxidative dehydrogenation under low-oxygen conditions

Yuan Ma,[a] Chaojun Guo,[a] Chuli Shi,[a] Yang Yang,[a] Shuobin Fu,[a] Baining Lin,[b] and Yonghua Zhou*[a]

[a] *College of Chemistry and Chemical Engineering, Central South University, Changsha 410083, China*

[b] *State Key Laboratory of Utilization of Woody Oil Resource, Hunan Academy of Forestry, Changsha 410004, China*

* Correspondence: zhouyonghua@csu.edu.cn.

List of Supporting Information：

The electron transfer within Pt-Zr on the surface of Al_2O_3

As shown in Fig. S1(a), due to the relatively slow reaction rate, both Pt/Al_2O_3 and $Pt\text{-}Zr/Al_2O_3$ exhibited a continuous induction period during the 56-hour reaction. In contrast, Zr/Al_2O_3 showed a 30-hour induction period and an 18-hour stability period, after which the X_{EB} declined while the S_{ST} stabilized. The X_{EB} and S_{ST} of the three catalysts at the 30th hour of the reaction and the C_{coke} after 56 hours of reaction are presented in Table S1 ($Pt\text{-}Zr/Al_2O_3$ and Zr/Al_2O_3) and Table 1 (Pt/Al_2O_3)**.** The TGA curves are depicted in Fig. S4. Among Pt/Al_2O_3, Zr/Al_2O_3, and $Pt\text{-}Zr/Al_2O_3$ catalysts, Zr/Al_2O_3 exhibited the highest X_{EB} (54.6%) and the lowest C_{coke} (5.1%); however, it showed the lowest S_{ST} (86.0%), with benzene as the main by-product. Pt/Al_2O_3 showed the opposite trend: the lowest X_{EB} (25.7%), highest C_{coke} (12.8%), and highest S_{ST} (97.0 %). The $Pt\text{-}Zr/Al_2O_3$ catalyst exhibited intermediate behavior, with a S_{ST} of 96.1%, significantly higher than that of Zr/Al_2O_3 due to Pt-Zr interaction. Its X_{EB} (33.1%) was higher than that of Pt/Al_2O_3. In comparison, its C_{coke} (11.3%) was lower, demonstrating that Zr addition improves the coke resistance of the Pt-based catalyst and enhances the catalytic activity slightly.

H_2-TPR and XPS examined the influence of Pt-Zr interaction on the catalyst properties. H_2-TPR analysis was only applied to Pt/Al_2O_3 and $Pt\text{-}Zr/Al_2O_3$, as ZrO_2 itself is not reducible. Fig. S1(b) reveals a single reduction peak for both catalysts, assigned to the reduction of PtO_x species. However, the peak for $Pt\text{-}Zr/Al_2O_3$ appears at a significantly higher temperature (243 °C) than that for Pt/Al_2O_3 (160 °C). An elevated reduction temperature typically signifies stronger metal-support interaction and improved metal dispersion.[S1]

The Zr 3d spectra (Fig. S1(c)) reveal an upward shift in the binding energy of Zr^{4+} in $Pt\text{-}Zr/Al_2O_3$ (182.4, 184.8 eV) compared to that in Zr/Al_2O_3 (182.2, 184.6 eV), indicating that Zr loses electrons in $Pt\text{-}Zr/Al_2O_3$. Conversely, the Pt 4d spectrum of $Pt\text{-}Zr/Al_2O_3$ (Fig. S1(d)) exhibits a shift to lower binding energy compared to Pt/Al_2O_3, suggesting electron enrichment on Pt. These complementary shifts provide clear evidence of an electron transfer from Zr to Pt, induced by their interaction.

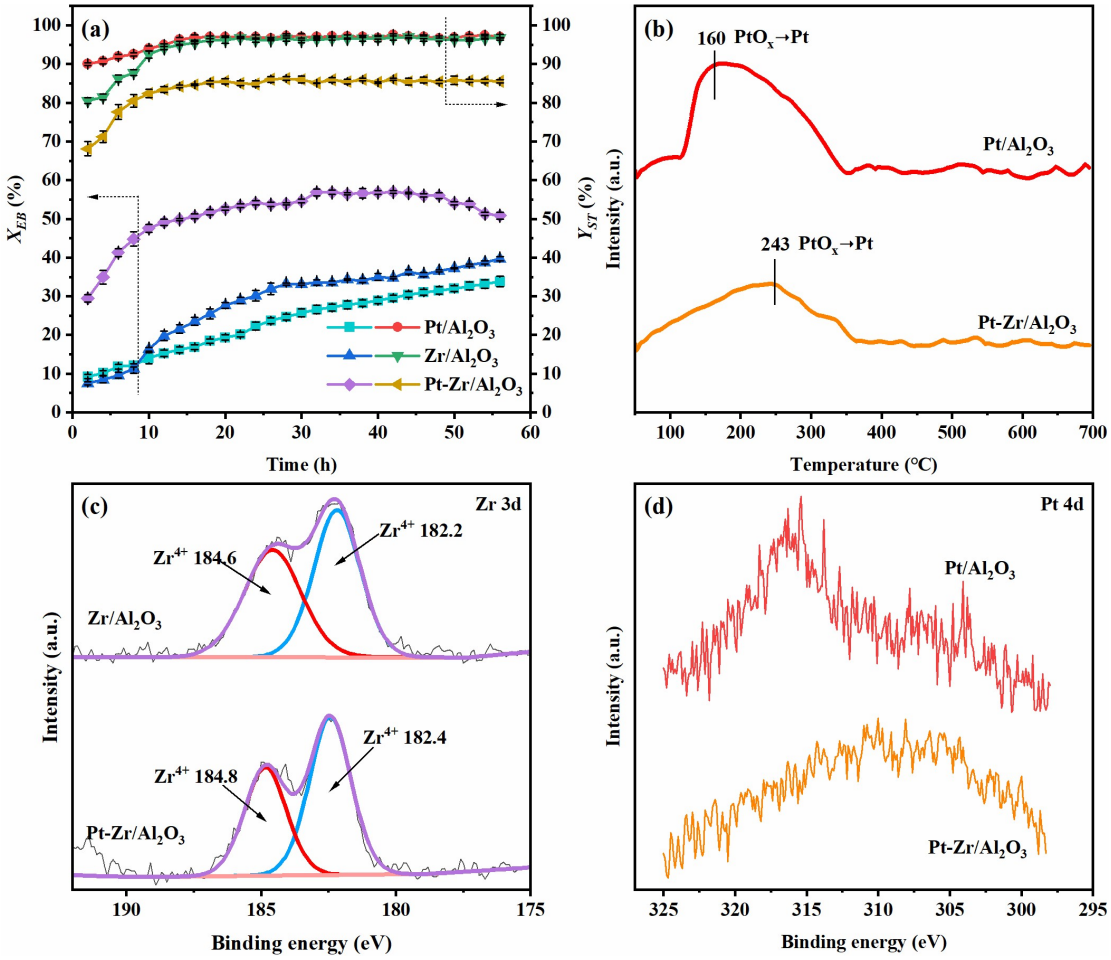

Fig. S1 Catalytic performance of Pt/Al_2O_3, Zr/Al_2O_3, and $Pt\text{-}Zr/Al_2O_3$ (a); H_2-TPR profiles of Pt/Al_2O_3 and $Pt\text{-}Zr/Al_2O_3$ (b); Zr 3d (c) and Pt 4d (d) in XPS spectra of Pt/Al_2O_3, Zr/Al_2O_3, and $Pt\text{-}Zr/Al_2O_3$. Reaction conditions: 0.4g catalyst, T = 600°C, 14.1 vol% ethylbenzene in N_2 (12 mL/min) and 5% O_2/N_2 (30mL/min).

Table S1. X_{EB} and S_{ST} of Zr/Al_2O_3, $Pt\text{-}Zr/Al_2O_3$, and $Fe\text{-}Zr/Al_2O_3$ catalysts at the 30th hour of reaction, C_{coke} after 56 hours of reaction, and Fe^{3+} content of fresh $Fe\text{-}Zr/Al_2O_3$.

Catalyst	X_{EB} (%)	S_{ST} (%)	C_{coke} [a] (%)	Fe^{3+}(%)	
				Fresh [b]	Used [b]
Zr/Al_2O_3	54.6	86.0	5.1	/	/
$Pt\text{-}Zr/Al_2O_3$	33.1	96.1	11.3	/	/
$Fe\text{-}Zr/Al_2O_3$	39.2	90.0	9.4	34.1	/

[a] Calculated from TGA results in Fig. S4.

[b] Calculated from Fe 2p XPS results in Fig S2(b).

The electron transfer within Fe-Zr on the surface of Al_2O_3

The catalytic performance of Fe/Al_2O_3, Zr/Al_2O_3, and $Fe\text{-}Zr/Al_2O_3$ in the ODH of ethylbenzene under low-oxygen conditions is shown in Fig. S2(a). It can be observed that after a 12-hour induction period, Fe/Al_2O_3 exhibits relatively stable activity. The X_{EB} is around 26–28%, and the S_{ST} lies between 96% and 98%. For $Fe\text{-}Zr/Al_2O_3$, the induction period is even longer: the X_{EB} increases gradually during the first 40 hours and then stabilizes, while the S_{ST} lies between 89% and 91%. Compared with Zr/Al_2O_3 and $Fe\text{-}Zr/Al_2O_3$, Fe/Al_2O_3 exhibits the lowest X_{EB} (26.8%), the highest C_{coke} (13.1%), and the highest S_{ST} (97.3%), as shown in Table 1. Due to the interaction between Fe and Zr, the $Fe\text{-}Zr/Al_2O_3$ catalyst exhibits intermediate values: 39.2% X_{EB}, 90.0% S_{ST}, and 9.4% C_{coke}, suggesting that the introduction of ZrO_2 significantly improves the coke resistance of the Fe-based catalyst but limits the selectivity.

As shown in the H_2-TPR profiles (Fig. S2(b)), both catalysts display three distinct reduction peaks. The low-temperature peak corresponds to the reduction of Fe_2O_3 to Fe_3O_4, the medium-temperature peak to the reduction of Fe_3O_4 to FeO, and the high-temperature peak to the reduction of FeO to metallic Fe. Notably, all three reduction peaks for $Fe\text{-}Zr/Al_2O_3$ appear at higher temperatures than those for Fe/Al_2O_3, suggesting that the Fe-Zr interaction inhibits the reduction of iron oxide. In addition, the content of the Fe^{3+} reduction peak in $Fe\text{-}Zr/Al_2O_3$ (13%) is higher than that in Fe/Al_2O_3 (8%).

The Zr 3d spectrum (Fig. S2(c)) shows that the binding energies of Zr^{4+} in $Fe\text{-}Zr/Al_2O_3$ are 182.1 eV and 184.4 eV, slightly lower than those in Zr/Al_2O_3 (182.2 eV and 184.6 eV), indicating an increase in electron density on Zr in the bimetallic catalyst. In the Fe 2p spectrum of $Fe\text{-}Zr/Al_2O_3$ (Fig. S2(d)), the binding energies of Fe^{2+} (711.1 eV) and Fe^{3+} (714.6 eV) shift to higher values relative to those in Fe/Al_2O_3 (710.9, 714.5 eV), suggesting a decrease in electron density on Fe. These results clearly demonstrate that the Fe-Zr interaction induces electron transfer from Fe to Zr, reducing the electron density of Fe and increasing that of Zr. This variation in electron density influences the Fe^{3+} content, as summarized in Table 1 and Table S1. The Fe^{3+} content in $Fe\text{-}Zr/Al_2O_3$ (34.1%, Table S1) is higher than that in Fe/Al_2O_3 (31.7%, Table 1), consistent with the

H_2-TPR results (Fig. S2(b)). Therefore, it can be concluded that the interaction between Fe and Zr not only facilitates the formation of Fe^{3+} but also suppresses its reduction.

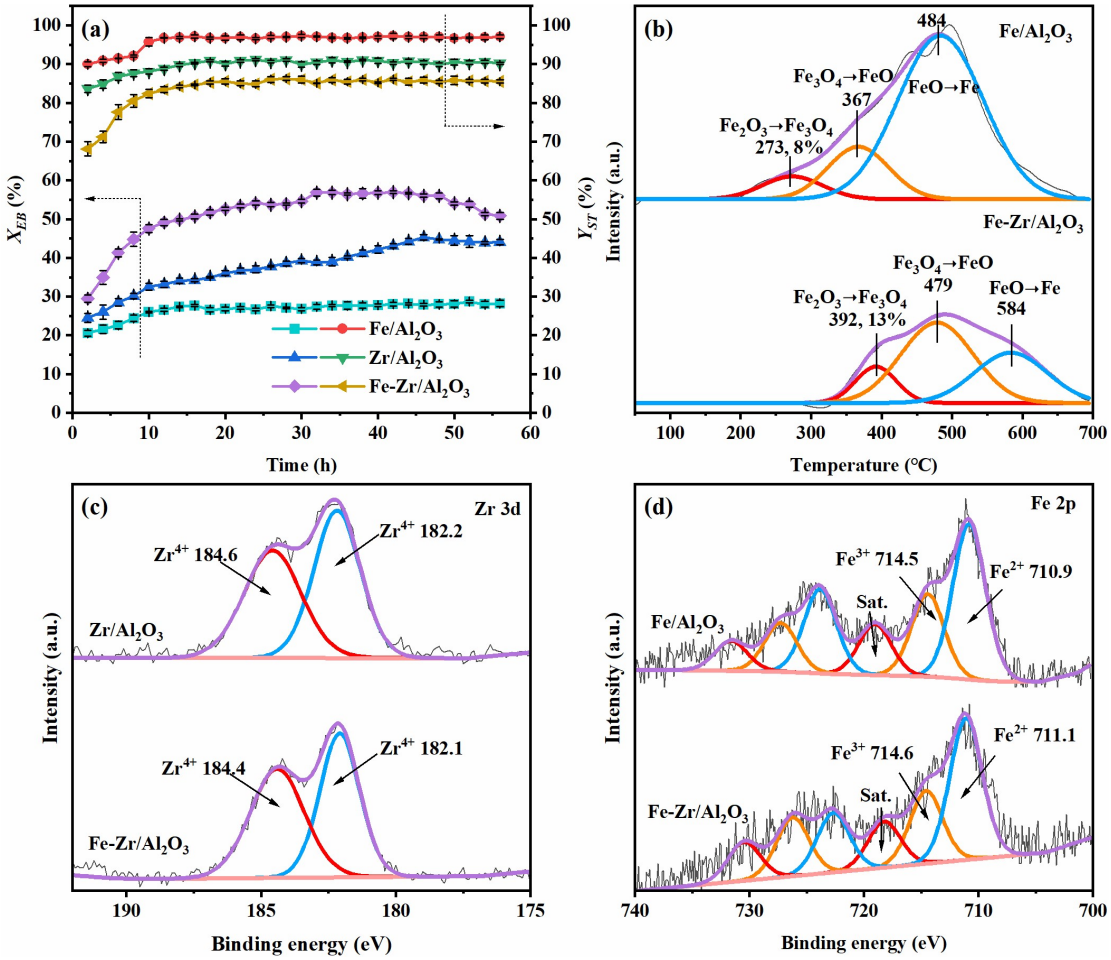

Fig. S2 Catalytic performance of Fe/Al_2O_3, Zr/Al_2O_3, and $Fe\text{-}Zr/Al_2O_3$ (a); H_2-TPR profiles of Fe/Al_2O_3 and $Fe\text{-}Zr/Al_2O_3$ (b); Zr 3d (c) and Fe 2p (d) in XPS spectra of Fe/Al_2O_3, Zr/Al_2O_3, and $Fe\text{-}Zr/Al_2O_3$. Reaction conditions: 0.4g catalyst, T = 600°C, 14.1 vol% ethylbenzene in N_2 (12 mL/min) and 5% O_2/N_2 (30mL/min).

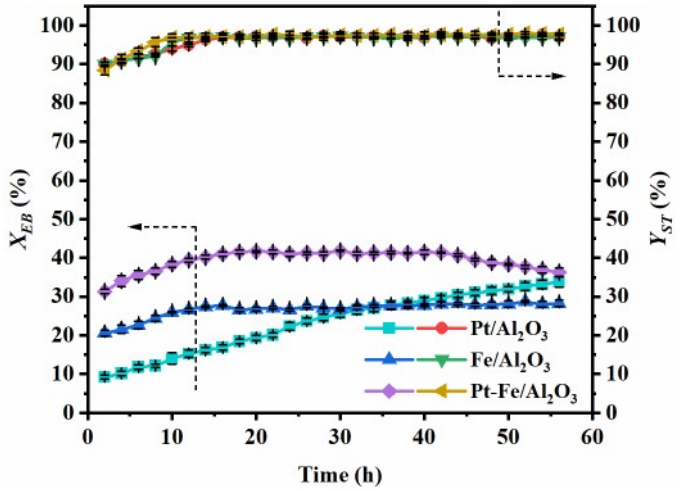

Fig. S3 Catalytic performance of Pt/Al_2O_3, Fe/Al_2O_3, and $Pt\text{-}Fe/Al_2O_3$.

Reaction conditions: 0.4g catalyst, T = 600℃, 14.1 vol% ethylbenzene in N_2 (12 mL/min) and 5% O_2/N_2 (30mL/min).

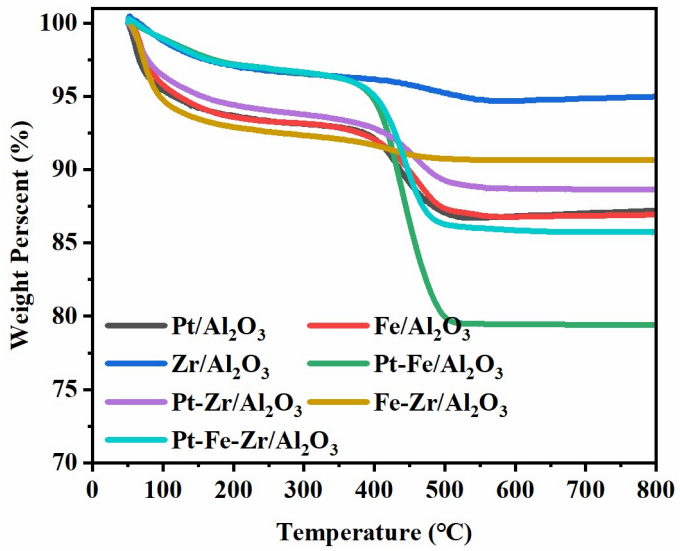

Fig. S4 TGA curves of different catalysts after a 56-hour reaction.

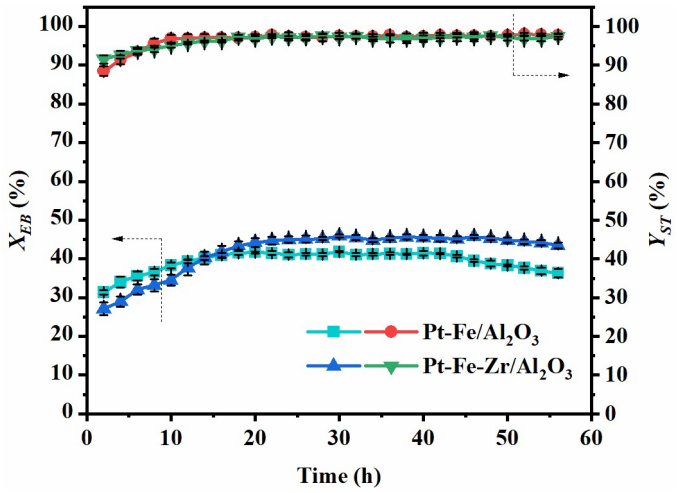

Fig. S5 Catalytic performance of Pt-Fe/Al_2O_3 and Pt-Fe-Zr/Al_2O_3.

Reaction conditions: 0.4g catalyst, T = 600℃, 14.1 vol% ethylbenzene in N_2 (12 mL/min) and 5% O_2/N_2 (30mL/min).

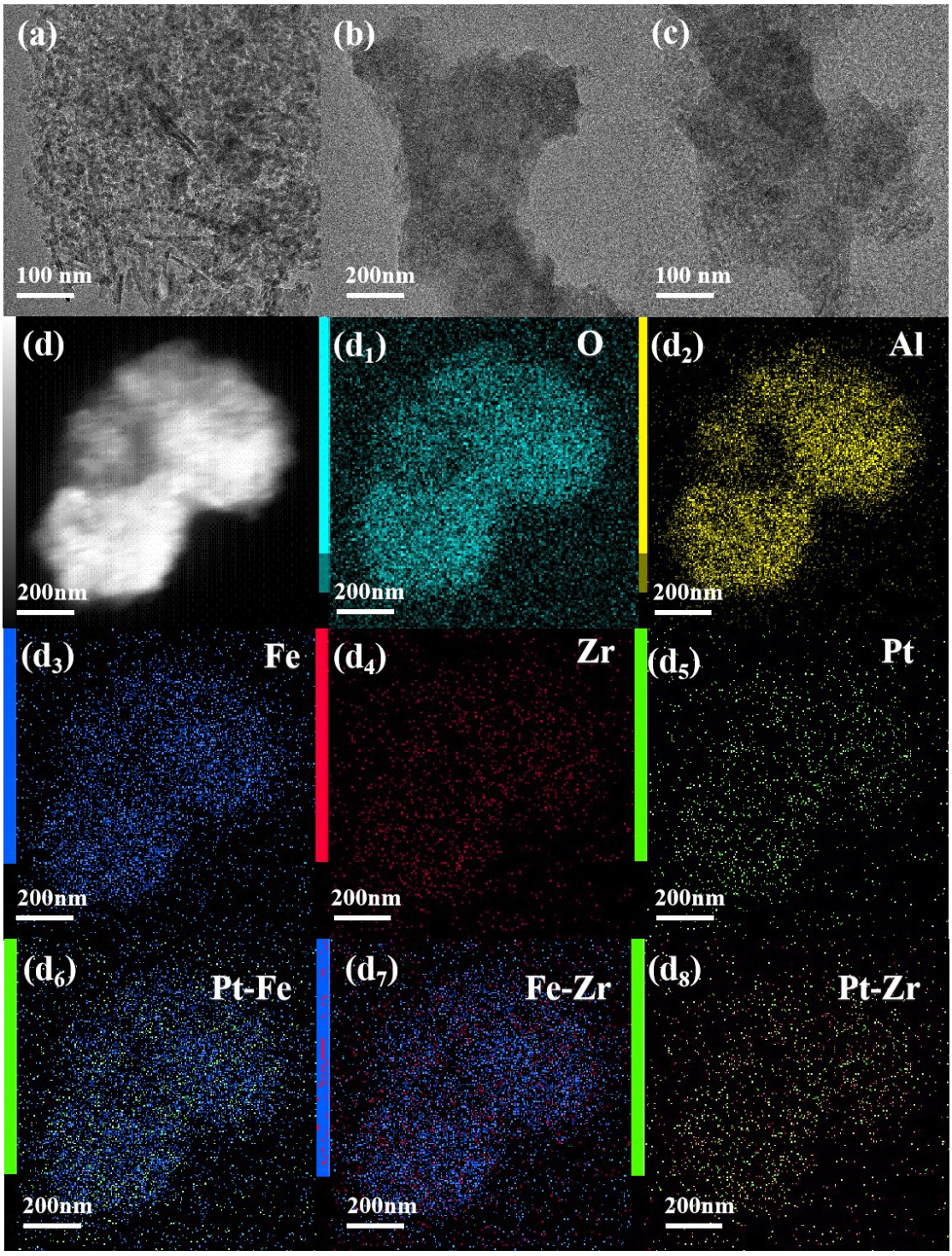

Fig. S6 TEM images of Al_2O_3 (a) and Pt-Fe-Zr/Al_2O_3 (b, c), along with element mapping images of Pt-Fe-Zr/Al_2O_3 (d, d_1–d_8).

Table S2. Comparison of various catalysts for ODH of ethylbenzene under low-oxygen conditions.

Catalyst	Reaction condition	Catalytic Performance			Reference
		X_{EB} (%)	S_{ST} (%)	Styrene production rate ($mmol.g^{-1}h^{-1}$)	
Pt-Fe-Zr/Al_2O_3	0.4g cat, 600°C, 14.1% EB in 12 mL min^{-1} N_2, O_2:EB=0.9	45.9	97.2	5.1	This work
Al_2O_3	0.5g cat, 450°C, 1.0g/h EB, O_2:EB=0.2	14.0	88.0	2.3	5
P_2O_5/Al_2O_3	0.5g cat, 500°C, 1.0g/h EB, O_2:EB=0.2	23.0	94.0	4.1	5
NDs	50mg cat, 450°C, 2.8% EB in 10 mL min^{-1} He, O_2:EB=0.1	27.0	96.5	4.0	8
15K-CeO_2	0.5g cat, 500°C, 0.5mL/h EB, N_2O:EB=3	69.0	82.0	4.6	11
BPO_4/BN	0.1g cat, 500°C, 5.6% EB in 10 mL min^{-1} N_2, O_2:EB=1.0	27.7	95.0	4.0	13
$Cr_{0.75}Fe_{1.25}O_3$,	0.1g cat, 590°C, 1.9mmol/h EB, 58.7 mmol/h CO_2	/	/	0.2	19
$MgFe_{0.1}Al_{1.9}O_4$	0.6 cat, 600°C, 9.8mmol/h EB, 49.2 mmol/h CO_2	97.5	92.3	4.2	S2

References

S1 C. Li, B. He, Y. Ling, C.-W. Tsang and C. Liang, *Chin. J. Catal.*, 2018, **39**, 1121–1128.

S2 M. Ji, X. Zhang, J. Wang, S. Park, *J. Mol. Catal. A-Chem.*, 2013, **371**, 36–41.